Journal of Engineering Mathematics **30:** 471–486, 1996.

Stationary circular target patterns in a surface burning reaction

LARRY K. FORBES
Department of Mathematics, University of Queensland, St. Lucia, Queensland 4072, Australia

Received 28 February 1995; accepted in revised form 30 August 1995

Abstract.
A simple model for burning on the circular face of a substrate is analyzed. It is shown that spatial patterns can form, in which the temperature develops hot and cold regions arranged in concentric circular rings. A linearized study shows the parameter values for which small amplitude patterns are stable. The fully non-linear equations are then solved using an efficient shooting method in the spatial variable, and an extremely complicated bifurcation diagram is obtained, from which it follows that multiple solutions occur at the same values of the defining parameters. The effect of heat leakage at the edges of the circular region is considered, and complicated non-linear behaviour occurs in this case also. Seven different temperature patterns, all co-existing at the same parameter values, are presented in a particular instance.
Key words: Exothermic reaction, pattern formation, multiple solutions, shooting method, bifurcation diagrams.

1. Introduction

The study of temperature sensitive chemical reactions is central to combustion theory, and it is now known that such reactions can exhibit an extraordinary range of dynamical behaviour. One of the first model combustion systems capable of exhibiting spontaneous oscillations in temperature was proposed by Sal'nikov [1] in 1949, and consists simply of two first-order decay reactions, at least one of which is exothermic. The temporal dynamics of this reaction, when well stirred, have been analyzed in detail by Gray and Roberts [2] and Forbes, Myerscough and Gray [3], for example, and a recent article by Gray and Forbes [4] demonstrates the full complexity of this apparently simple scheme, when both decay reactions involve temperature dependent reaction rates.

Although the Sal'nikov reaction was originally proposed as a mathematical model, to illustrate the possibility of spontaneous oscillations, it has nevertheless been shown to have significant application to real combustion systems. Gray and Griffiths [5] found reasonable agreement between the oscillatory behaviour predicted by the Sal'nikov model and experimental observations for a reaction involving gaseous di tert-butyl peroxide. The oscillatory behaviour of the hydrogen-chlorine reaction has also been studied in relation to the predictions of the Sal'nikov model, in a thorough investigation by Coppersthwaite, Griffiths and Gray [6], and agreement with measured temperature histories was obtained.

If the reaction domain is not well mixed, then spatial patterns are possible, in addition to the temporal oscillations that can occur. From a mathematical point of view, the spatially homogeneous steady state becomes unstable as a result of the combined effects of reaction and diffusion, and a spatial pattern is formed by means of a Turing bifurcation. Some general properties of Turing patterns are discussed by Dillon, Maini and Othmer [7], for example. Small amplitude Turing patterns in the simple Sal'nikov model of combustion are investigated

by Gray and Scott [8] (chapter 10), and have been continued numerically to large amplitude by Forbes [9] using a spectral solution method. In this case, multiple solutions were found to be possible, and their stability was assessed by means of an eigenvalue analysis.

In addition to stationary patterns, it is of course the case that other important spatially varying structures can form in a combustion system. Travelling waves were examined by Gray and Kordylewski [10] for a particularly simple exothermic reaction, and an extension of this model to include the effects of species consumption has been used recently by Bayliss, Matkowsky and Riecke [11], to study travelling waves in cellular flames. Bayliss and Matkowsky [12] argue that, when heat loss at the wall is taken into account, solutions may be obtained which are apparently chaotic.

In the present paper, the simple reaction scheme of Sal'nikov [1] is used, as a model for burning at the face of a circular substrate. In view of the demonstrated relevance of this model particularly to gas-phase reactions, the problem to be studied here is essentially the formation of spatial patterns in combustion at the nozzle of an oxy-welder, for example, and direct Newtonian cooling to ambient temperature at the reaction face is permitted in the model. The chemical scheme is simply

$$S \xrightarrow{k_0} C \xrightarrow{k_1} P, \tag{1}$$

in which S denotes the substrate, C is some intermediate chemical produced by the two-stage decay process, and P is an inert product which is removed from the reaction zone. The feeder rate k_0 is assumed to be constant, but the second rate parameter k_1 is temperature dependent, according to Arrhenius kinetics, and has the form

$$k_1(T) = M_1 \exp(-E/RT). \tag{2}$$

Here, M_1 is a constant having units time^{-1}, the activation energy for the reaction is E, R is the universal gas constant and T denotes temperature.

The rate law for intermediate product C is obtained simply from the first order reaction scheme (1) and may be written

$$\frac{\partial [C]}{\partial t} = D\nabla^2[C] + k_0[S] - k_1[C], \tag{3}$$

where D represents the diffusion coefficient for the chemical C, and the square brackets [] denote the molar concentration of the relevant species.

In view of the fact that rate parameter k_1 is temperature sensitive, it is necessary to express conservation of heat energy at every point on the reaction surface by means of the equation

$$\rho c_h \frac{\partial T}{\partial t} = K\nabla^2 T - \chi(T - T_a) + Q_1 k_1[C]. \tag{4}$$

The quantities ρ and c_h are respectively the density and heat capacity of the substrate, and the first term on the right hand side, with heat conduction constant K, represents the diffusion of heat energy according to Fourier's law of conduction. The second term on the right allows for Newtonian cooling, at constant rate χ, to ambient temperature T_a, and the last term represents the heat produced by the second (exothermic) stage of reaction scheme (1). A detailed derivation of equation (4) is given in Forbes [9]. Finally, the system (2)–(4) is supplemented by zero-flux boundary conditions

$$\frac{\partial [C]}{\partial n} = \frac{\partial T}{\partial n} = 0 \tag{5}$$

at the perimeter of the circular region, $r = A$.

Dimensionless variables are defined, using $1/M_1$ as the unit of time, and the radius A of the reaction region as the length scale. Temperature is scaled relative to the ratio E/R, and the most convenient unit for concentration is the quantity $(\rho c_h E)/(Q_1 R)$. In terms of these new dimensionless variables, the governing equations (2)–(4) become

$$\begin{aligned} \frac{\partial C}{\partial t} &= \sigma \nabla^2 C + \mu - C e^{-1/T} \\ \frac{\partial T}{\partial t} &= \alpha \nabla^2 T - \beta(T - \theta_a) + C e^{-1/T}, \end{aligned} \tag{6}$$

with boundary conditions taken from equations (5), in the form

$$\partial C/\partial r = \partial T/\partial r = 0 \quad \text{on} \quad r = 1. \tag{7}$$

Solutions to these equations are dependent upon the five dimensionless constants $\sigma = D/(M_1 A^2)$ and $\alpha = K/(M_1 \rho c_h A^2)$ which are respectively the diffusion coefficient for chemical C and the dimensionless heat conduction, $\beta = \chi/(M_1 \rho c_h)$ the rate of Newtonian cooling at the reaction surface, the dimensionless ambient temperature $\theta_a = (RT_a)/E$, and the supply rate $\mu = (k_0[S]Q_1 R)/(M_1 \rho c_h E)$ of the substrate chemical S.

In the next section, a linearized theory for the system (6)–(7) is given, and shows the parameter regions within which stable stationary patterns are to be expected. An efficient shooting method for solving the steady equations is outlined in Section 3, and the results of extensive numerical calculation are outlined in Section 4. The effect of altering the boundary conditions (7) to allow heat loss at the circumference of the circular burning region is considered in Section 5, and reveals a highly complex bifurcation structure, in which many different patterns can co-exist.

2. The linearized solution

In this section, a small amplitude solution for spatial patterns is outlined, and reveals the region of the parameter space where stable steady-state patterns are to be expected. This solution is then used as the basis of the numerical work in following sections.

The concentration $C(r,t)$ and temperature $T(r,t)$ in equations (6) are expanded in perturbation series

$$\begin{aligned} C(r,t) &= C_e + \epsilon C_1(r,t) + O(\epsilon^2) \\ T(r,t) &= T_e + \epsilon T_1(r,t) + O(\epsilon^2), \end{aligned} \tag{8}$$

and terms are collected at each order of the parameter ϵ, which is essentially a measure of the pattern amplitude.

At zeroth order in pattern amplitude ϵ, the equilibrium concentration C_e and temperature T_e are found to be

$$C_e = \mu e^{1/T_e} \quad \text{with} \quad T_e = \theta_a + \mu/\beta \tag{9}$$

The linearized equations, of primary interest in this section, are obtained by collecting terms of first order in amplitude ϵ. These are most conveniently expressed in vector form, by

creating the vector function $\mathbf{U_1} = [C_1, T_1]^T$, containing the first-order correction functions defined in the perturbation scheme (8). The equations may then be written

$$\frac{\partial \mathbf{U_1}}{\partial t} = \mathbf{D_m}\left(\frac{\partial^2 \mathbf{U_1}}{\partial r^2} + \frac{1}{r}\frac{\partial \mathbf{U_1}}{\partial r}\right) + \mathbf{A}\mathbf{U_1} \tag{10}$$

subject to boundary conditions

$$\partial \mathbf{U_1}/\partial r = \mathbf{0} \quad \text{on} \quad r = 1. \tag{11}$$

Here, a matrix of diffusion coefficients

$$\mathbf{D_m} = \begin{pmatrix} \sigma_m & 0 \\ 0 & \alpha \end{pmatrix}$$

has been defined, and the subscript m refers to the fact that, for steady patterns, the coefficient σ is determined as an eigenvalue in a problem for which the vector $\mathbf{U_1}$ is the associated eigenfunction. In addition, the matrix $\mathbf{A}$ is

$$\mathbf{A} = \begin{pmatrix} -\exp(-1/T_e) & -\mu/T_e^2 \\ \exp(-1/T_e) & -\beta + \mu/T_e^2 \end{pmatrix},$$

and the equilibrium quantities C_e and T_e are given in (9).

The steady-state solution to the linearized equations (10), satisfying the boundary conditions (11), must be sought in the form

$$\mathbf{U_1}(r) = \mathbf{B}J_0(j_{1,m}r), \tag{12}$$

where J_0 denotes the Bessel function of first kind and order zero, and the constants $j_{1,m}$ are the zeros of the Bessel function J_1 of order one. When the form of the pattern (12) is substituted into the governing equations (10), the equation

$$\mathbf{AB} = j_{1,m}^2 \mathbf{D_m B}$$

is obtained, which is evidently a (generalized) eigenvalue problem for the diffusion coefficient σ, with $\mathbf{B}$ as the associated eigenvector. After a little algebra, the eigenvalue is obtained in the form

$$\sigma_m = \frac{T_e^2(\beta + j_{1,m}^2\alpha)\exp(-1/T_e)}{j_{1,m}^2[\mu - T_e^2(\beta + j_{1,m}^2\alpha)]} \tag{13}$$

which is similar to the expression for one-dimensional patterns found by Forbes [9].

In view of the physical requirement that the diffusion coefficient (13) must be positive, it follows simply that

$$\alpha < \frac{1}{j_{1,m}^2}\left(\frac{\mu}{T_e^2} - \beta\right). \tag{14}$$

Similarly, the heat conduction coefficient α in equation (14) must also be positive, which gives the condition

$$\theta_a < \sqrt{\mu/\beta} - \mu/\beta \tag{15}$$

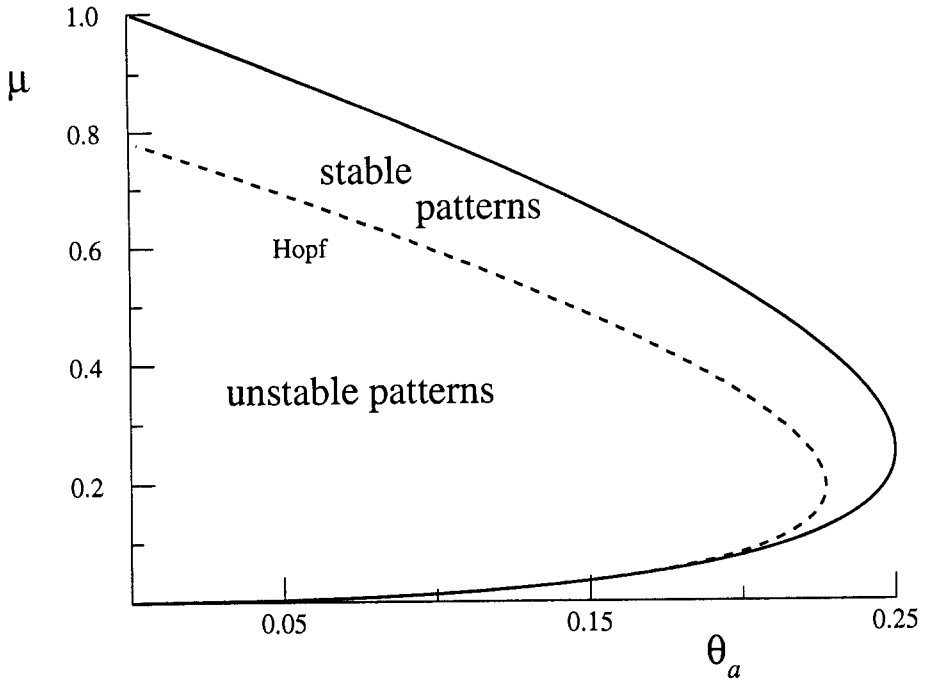

Fig. 1. The region of the parameter space within which patterns can be formed for $\beta = 1$. The dashed line labelled 'Hopf' is the boundary between stable and unstable patterns; in the well mixed problem, it gives the location of Hopf bifurcations at which spontaneous oscillatory combustion (in time) is generated.

for patterns to be formed. This is sketched in Figure 1 as the upper (solid) line. Since the ambient temperature θ_a in condition (15) must also be positive, it follows that patterns can only be formed if $\mu < \beta$.

Stability of the stationary patterns (12) can be studied in the linearized approximation by considering the time-dependent problem (10), subject to the zero-flux boundary conditions (11), and with diffusion coefficient σ given as one of the eigenvalues (13). It is evident that the solution varies with time t according to the general formula

$$\mathbf{U_1}(r,t) = \sum_{q=0}^{\infty}\sum_{r=1}^{2} \mathbf{K_{q,r}} J_0(j_{1,q}r)\exp(\lambda_{q,r}t)$$

in which the exponents $\lambda_{q,r}$ are obtained as the eigenvalues of the matrix equations

$$[\mathbf{A} - j_{1,q}^2\mathbf{D_m}]\mathbf{K_{q,r}} = \lambda_{q,r}\mathbf{K_{q,r}}, \quad q = 0,1,2,\ldots \tag{16}$$

When written out in full, the eigenvalue equation (16) gives rise to a quadratic expression for $\lambda_{q,r}$, which can be represented as

$$\lambda_{q,r}^2 - \Sigma_{m,q}\lambda_{q,r} + \Delta_{m,q} = 0, \tag{17}$$

in which the trace and determinant of the matrix on the left-hand side of equation (16) are

$$\begin{aligned}\Sigma_{m,q} &= -j_{1,q}^2(\sigma_m + \alpha) - (\beta - \mu/T_e^2 + e^{-1/T_e}) \\ \Delta_{m,q} &= j_{1,q}^4\sigma_m\alpha + j_{1,q}^2[\alpha e^{-1/T_e} + \sigma_m(\beta - \mu/T_e^2)] + \beta e^{-1/T_e}.\end{aligned} \tag{18}$$

A necessary condition for the stability of the steady-state patterns (12) is therefore that the real part of the eigenvalues $\lambda_{q,r}$ should be negative, for all $q = 0,1,2,\ldots$ and $r = 1,2$. Equivalently, the trace $\Sigma_{m,q}$ must be negative, from which it follows that

$$\beta - \mu/T_e^2 + e^{-1/T_e} > 0 \tag{19}$$

is necessary for pattern stability in the linearized analysis. This condition is also illustrated in Figure 1, by means of the dashed line labelled 'Hopf' on the diagram.

Patterns are therefore possible within the parameter region allowed by condition (15); inside this region, patterns are stable if they conform with inequality (19), and unstable otherwise. This information is represented in Figure 1. It is also possible to give a clear physical interpretation for condition (19), since the stability or otherwise of the spatial patterns is related to the emergence of spontaneous oscillations in the well mixed reaction. Condition (19), when obeyed as an equality, is precisely the curve in the parameter plane along which time dependent oscillations can be born by means of a Hopf bifurcation from the homogeneous steady state. Inside the region enclosed by the dashed curve in Figure 1, where the patterns are unstable, the well mixed reaction exhibits spontaneous oscillatory combustion, but no such oscillations occur outside this region, at least in small amplitude theory. Consequently, spatial patterns exist as time dependent standing waves within the parameter region enclosed by the dashed curve, but as stable time independent structures outside this region.

3. Numerical solutions for steady state patterns

Solutions of very great accuracy have been obtained, for time independent patterns, using an efficient shooting method. This approach yields results of far superior accuracy to spectral methods (e.g. [9]), and additionally requires only a fraction of the computing resources. Consequently, it is possible to explore a much larger region of the solution space with this method.

The radial coordinate r is represented by N equally spaced discrete points $r_j, j = 1,2,\ldots,N$, in such a way that $r_1 = 0$ and $r_N = 1$. An interior matching point r_m is chosen from this set, and we have found it convenient to use $r_m = 1/2$.

To begin the shooting algorithm, the parameters μ, β, θ_a and α are all specified. In addition, we give the temperature amplitude A_T of the pattern, defined here as

$$A_T = T(0) - T(1). \tag{20}$$

An initial guess is now made for the vector of unknowns

$$\mathbf{u} = [C_1, T_1, C_N, \sigma]^T, \tag{21}$$

the four elements of which are respectively the concentration and temperature at $r = 0$, the concentration at $r = 1$, and the diffusion coefficient σ.

With values assumed for the elements of the vector $\mathbf{u}$ in equation (21), a trial pattern is now computed. The governing equations (6), in steady-state form, are written as a system of four ordinary differential equations, by making the changes of variable

$$\psi_1 \equiv C_(r) \qquad \psi_2 \equiv C'(r)$$
$$\psi_3 \equiv T(r) \qquad \psi_4 \equiv T'(r)$$

For $r \neq 0$, the system to be solved therefore becomes

$$\begin{aligned}
\psi_1' &= \psi_2 \\
\psi_2' &= -\frac{\psi_2}{r} - \frac{1}{\sigma}[\mu - \psi_1 e^{-1/\psi_3}] \\
\psi_3' &= \psi_4 \\
\psi_4' &= -\frac{\psi_4}{r} + \frac{1}{\alpha}\left[\beta(\psi_3 - \theta_a) - \psi_1 e^{-1/\psi_3}\right].
\end{aligned} \tag{22a}$$

When $r = 0$, the term $(1/r)(\partial C/\partial r)$ in the polar form of the Laplacian operator in equations (6) can be replaced by the second derivative $\partial^2 C/\partial r^2$, and so, for $r = 0$, the second and fourth equations in the system (22a) are replaced by

$$\begin{aligned}
\psi_2' &= -\frac{1}{2\sigma}[\mu - \psi_1 e^{-1/\psi_3}] \\
\psi_4' &= \frac{1}{2\alpha}\left[\beta(\psi_3 - \theta_a) - \psi_1 e^{-1/\psi_3}\right].
\end{aligned} \tag{22b}$$

The standard fourth-order Runge-Kutta method is used to integrate the system (22) on the left-hand side of the matching point, from $r_1 = 0$ to $r = r_m$. The initial conditions for the numerical integration are $\psi_1 = C_1, \psi_2 = 0, \psi_3 = T_1$ and $\psi_4 = 0$, which follows from the guess (21) and the requirement of analyticity at the pattern centre $r = 0$. This gives values $C_{m,L}$, $C'_{m,L}$, $T_{m,L}$, and $T'_{m,L}$ at the left hand side of the matching point $r = r_m$.

A similar procedure is used on the right side of the matching point. Since the pattern amplitude A_T is known, the temperature T_N at $r = 1$ is given simply from equation (20) in the form $T_N = T_1 - A_T$. The Runge-Kutta method is now used to integrate backwards from $r = 1$ to the right-hand side of the matching point $r = r_m$, using starting values taken from the guess (21) and the boundary conditions (7) at the perimeter $r = 1$ of the reaction region. This yields values $C_{m,R}$, $C'_{m,R}$, $T_{m,R}$ and $T'_{m,R}$ at the right hand side of the matching point.

The values of concentration C and temperature T and their first derivatives on the left and right sides of the matching point $r = r_m$, will not, in general, be equal, and so Newton's method is used to adjust the guess (21) iteratively until equality is obtained. This is usually achieved in about five iterations, at which point a valid steady state pattern has been found. We typically use between 8000 and 64,000 numerical mesh points on either side of the matching point, and this guarantees at least eight decimal places of accuracy for the solution, in only several minutes of execution time on a 486 personal computer.

One disadvantage of the shooting method, when compared with spectral techniques, is that it does not readily yield information about the stability of the non-linear pattern. Nevertheless, it has been found by Forbes [9] that unstable one-dimensional burning patterns decay only slowly, so that stability is not of major concern. This was reinforced in a study of the Belousov-Zhabotinskii reaction [13], where direct time integration of the governing equations showed that unstable patterns would persist long enough for them to be observed comfortably in the laboratory. For this reason, the extreme accuracy and speed of the shooting method approach more than compensates for the lack of information about pattern stability.

4. Results for stationary insulated patterns

When the Newtonian cooling coefficent has the value $\beta = 1$, it is clear from Figure 1 that stable patterns are confined to a rather small region of the parameter space. For definiteness

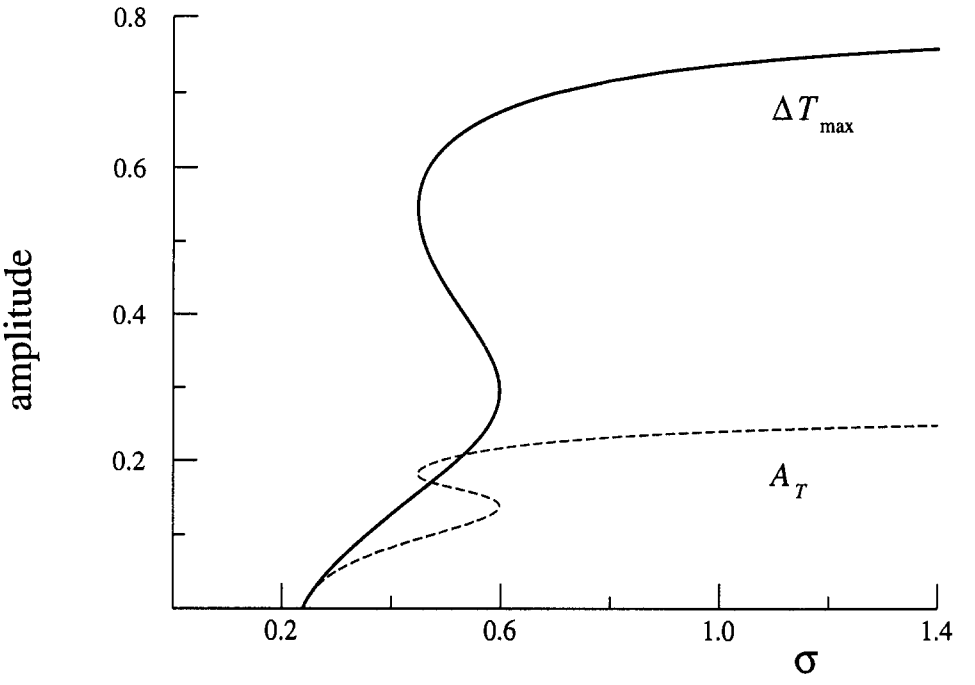

Fig. 2. Variation of pattern amplitude with diffusion coefficient σ, for the first eigensolution. Here, $\beta = 1$, $\alpha = 0.001$, $\mu = 0.5$ and $\theta = 0.18$.

in this section, it will be assumed that $\beta = 1$, with thermal conductivity coefficient $\alpha = 0.001$, reagent supply rate $\mu = 0.5$ and ambient temperature $\theta_a = 0.18$. These values are within the region where the linearized solution of section 2 is stable, and appear to give results indicative of other parameter values within this zone.

It follows from equation (13) that the diffusion coefficient for small amplitude patterns is only positive, for these parameter values, when $m < 3$. We shall therefore be concerned only with the first two eigenmodes in the formation of burning patterns, and equation (13) indicates that the chemical diffusion coefficients (the eigenvalue) for these two modes are $\sigma_1 = 0.2383$ and $\sigma_2 = 0.1526$. Higher modes are not of physical interest, since they do not give a positive eigenvalue.

Figure 2 shows a bifurcation diagram for the first eigensolution, $m = 1$. Here, the amplitude of the patterns A_T defined in equation (20) has been plotted as it varies with the diffusion coefficient σ, and is sketched with a dashed line on the diagram. This curve intersects the horizontal axis at the value $\sigma_1 = 0.2383$ predicted by the linearized analysis of Section 2. The results shown in this figure are compiled from 165 separate converged non-linear solutions to the system (22). It has also been useful to define another measure of pattern amplitude, given by ΔT_{max}, which is taken to be the difference between the maximum and minimum values of temperature across the pattern. This quantity is sketched with a solid line in Figure 2.

Both measures of amplitude in Figure 2, namely A_T and ΔT_{max}, increase as the diffusion coefficient σ is increased beyond the linearized value $\sigma_1 = 0.2383$. In fact, the curves continue beyond the right-hand side of the diagram to $\sigma \to \infty$, where $A_T \to 0.26687$ and $\Delta T_{max} \to 0.81574$; this information was determined with the present numerical method from a solution obtained with $\sigma = 10^7$. In this limit $\sigma \to \infty$, the first equation in the system (6) permits

only a constant solution for the concentration C in the steady state, so that the shape of the temperature profile is determined by the second equation in the system (6) (the energy equation) alone.

It is also evident from Figure 2 that there is a region in which three patterns exist simultaneously, in the approximate interval $0.44 < \sigma < 0.6$. It is likely that the smallest and largest amplitude patterns in this region are stable in time, and that the pattern of intermediate amplitude is unstable. There is therefore a genuine and interesting lack of uniqueness in solutions to this problem, and which of the patterns would actually be observed in the laboratory presumably depends on the initial conditions in the experiment.

Three different patterns are shown in Figure 3a, and were all computed with diffusion coefficient $\sigma = 0.5$. Each pattern has an extensive region of high temperature to the left of the diagram, near the centre $r = 0$ of the circular burning region, and a cooler region near the edge of the pattern, as evidenced by the dip in temperature to the right of the figure. To emphasize the fact that these are circular patterns, the largest amplitude solution in Figure 3a is drawn over the entire circular domain in Figure 3b. The region of high temperature at the centre is clearly visible, as is the dip in temperature near the edge of the region. Notice also that the profile becomes flat at the rim $r = 1$, as is required by the boundary conditions (7).

The second eigensolution is now investigated using the numerical shooting method of Section 3, and the results are displayed in Figures 4(a) and (b). In these diagrams, the curves have been plotted using 343 separate converged solutions to the system of equations (22), and the pattern amplitude A_T defined in equation (20) is shown in Figure 4(a), while the maximum measure of amplitude $\Delta T_{\max}$ is displayed in Figure 4(b).

It is evident from Figures 4(a) and (b) that the second eigensolution has an extremely elaborate bifurcation behaviour. It emerges from the linearized solution $\sigma_2 = 0.1526$ and begins to grow with increasing diffusion coefficient σ, before then undergoing a fold bifurcation to smaller values of σ. It folds again at about $\sigma = 0.06$ and moves towards the right before again folding at about $\sigma = 0.22$. The numerical results indicate that the amplitude A_T in Figure 4(a) forms a genuine cusp at this value, and a modified version of the numerical scheme in Section 3 was necessary to continue the solution around this point; it allowed the temperature $T(0)$ at $r = 0$ to be given, and both σ and A_T to be found numerically. A further fold bifurcation occurs at about $\sigma = 0.08$, before the solution branch eventually terminates on the horizontal axis, at $\sigma_1 = 0.2383$.

A second, and apparently unrelated, branch of solutions also bifurcates from the second eigenvalue $\sigma_2 = 0.1526$, and has been sketched with a dashed line in Figures 4(a) and (b). It also undergoes a fold bifurcation at about $\sigma = 0.046$ before turning and continuing out to the right of Figures 4. It seems likely that this solution branch will also continue to $\sigma \to \infty$, although it becomes extremely difficult to follow numerically, and its fate beyond about $\sigma = 0.48$ is therefore somewhat uncertain.

Figures 4(a), (b) also reveal the fact that the Turing bifurcation points $\sigma_1 = 0.2383$ and $\sigma_2 = 0.1526$, indicated with small open circles on each picture, have a complicated structure that allows multiple solution branches to bifurcate from each point. (This is a different behaviour from the Hopf bifurcation points seen in the generation of time dependent oscillations in well stirred combustion reactions, where only a single solution bifurcates from each point.) It has been seen that both a first eigenmode and a second eigenmode solution bifurcate from the point $\sigma_1 = 0.2383$, and that two different second eigenmode solutions have emerged from the point $\sigma_2 = 0.1526$. Whether additional solution branches also exist is unclear, although no extra have been found numerically.

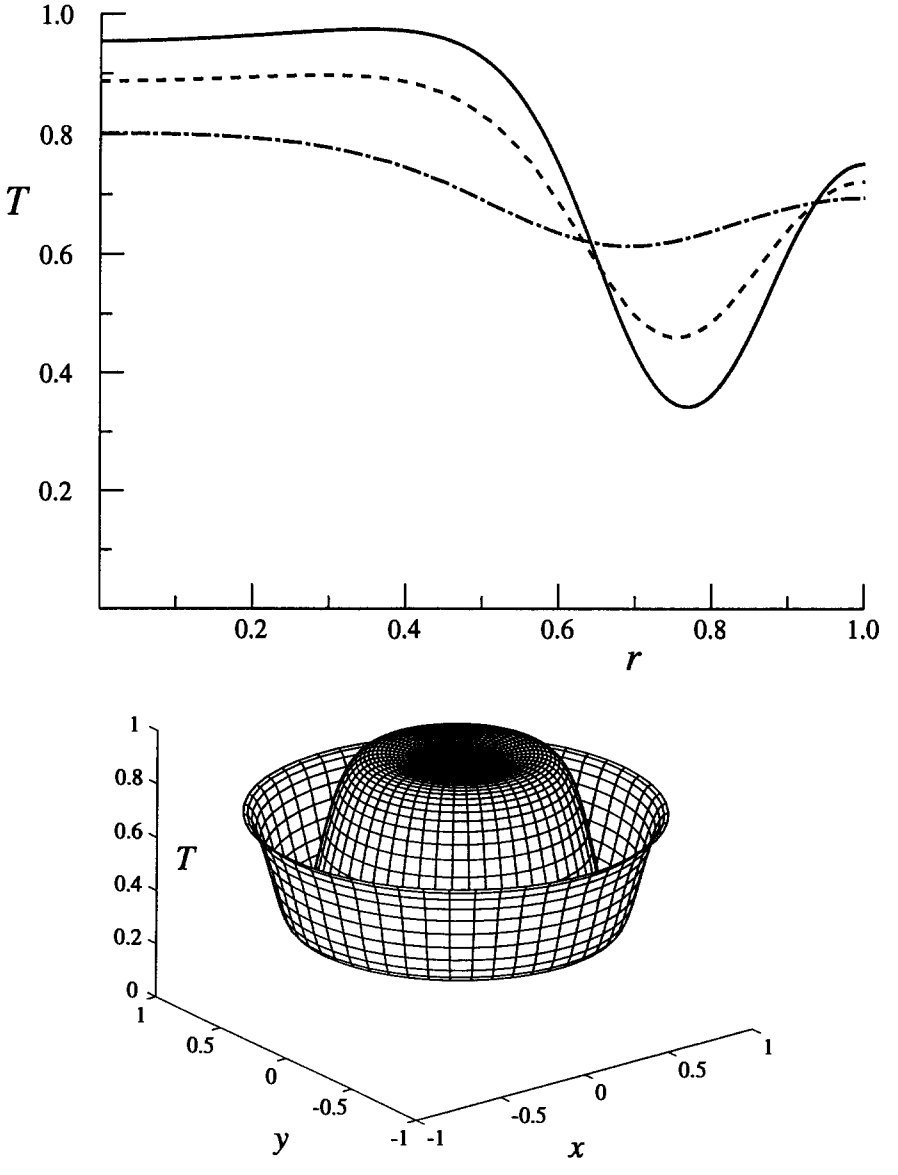

Fig. 3. (a) Three different patterns, all obtained with the same diffusion coefficient $\sigma = 0.5$. (b) Three dimensional view of the largest amplitude profile in part (a). The remaining parameters have the same values as for Figure 2.

Six different patterns, all computed at the same values of the governing parameters, are shown in Figures 5, for the value of diffusion coefficient $\sigma = 0.1$. The first four such patterns, corresponding to the curve sketched with a solid line in Figures 4, are displayed in Figure 5(a), and the two solutions in Figure 5(b) are taken from the second branch of solutions in Figures 4, sketched with a dashed line. These diagrams again illustrate the great complexity of pattern possibilities that arise in this problem, as a consequence of the inherent non-linearity of the system (6). Which of the patterns would actually be observed in an experiment would doubtless depend upon initial conditions.

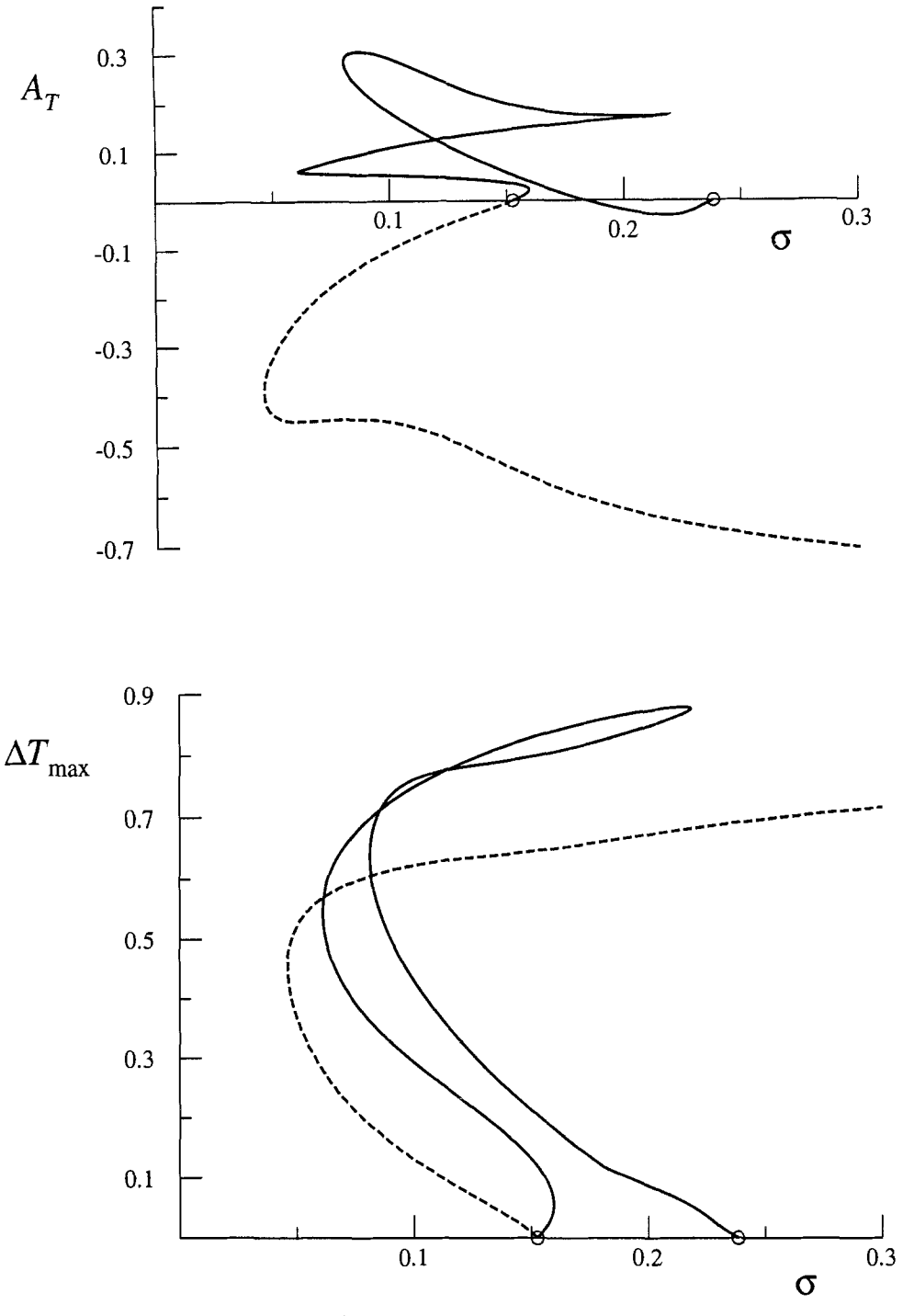

Fig. 4. Variation of pattern amplitudes (a) A_T and (b) ΔT_{max} with diffusion coefficient σ, for the second eigen-solution. Here, $\beta = 1$, $\alpha = 0.001$, $\mu = 0.5$ and $\theta_a = 0.18$. The small circles on the horizontal axis indicate the positions of the two Turing bifurcation points $\sigma_1 = 0.2383$ and $\sigma_2 = 0.1526$.

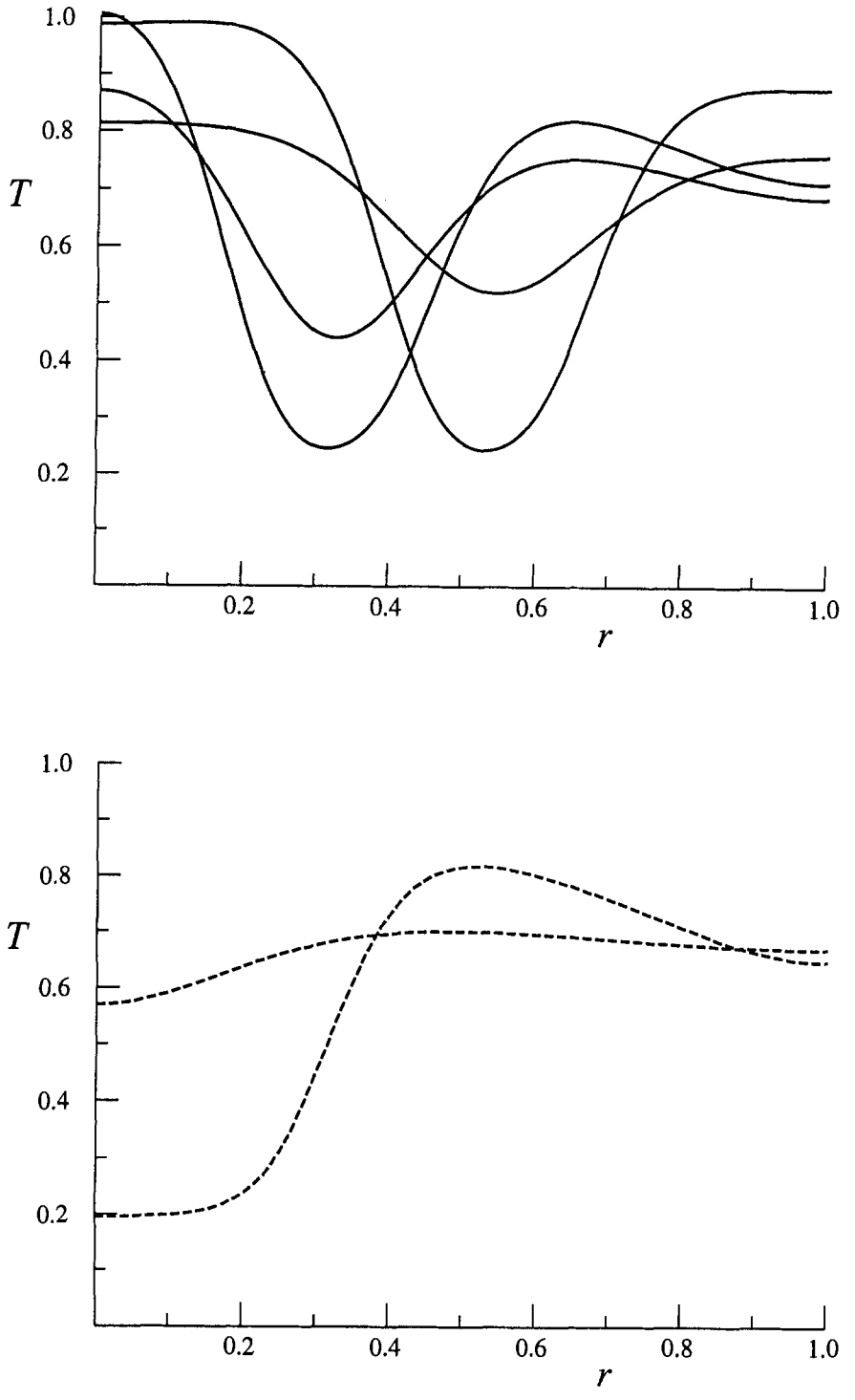

Fig. 5. (a) and (b). Six different patterns, all obtained with the same diffusion coefficient $\sigma = 0.1$. The remaining parameters have the same values as for Figure 4.

5. The effect of boundary heat loss

In real systems, it is unlikely that the boundary $r = 1$ would remain perfectly thermally insulated, and so it is appropriate to conclude this paper with a brief investigation of the effects of heat dissipation at the edge of the circular region. This is done by replacing the second of the boundary conditions (7) with the term

$$\partial T/\partial r = -\gamma(T - \theta_a) \quad \text{on} \quad r = 1. \tag{23}$$

Here, the positive constant γ represents the coefficient of cooling to ambient temperature θ_a at the boundary.

It is possible to perform a linearized analysis in the case of boundary heat loss $\gamma \neq 0$, exactly as in Section 2, provided that the coefficient γ is small. In addition to the perturbation expansions (8), it is therefore necessary to set

$$\gamma = \epsilon\gamma_1 + O(\epsilon^2),$$

with small parameter ϵ measuring the pattern amplitude, as before. The details are reasonably straightforward, and so will not be given here, but the significant qualitative difference between this result and the solution of Section 2 is that, when γ_1 is not zero, patterns are no longer obtained as solutions to an eigenvalue problem. Whereas in Section 2, linearized patterns could only be obtained at the special values of diffusion coefficient σ given by the formula (13) and the amplitude remained arbitary, when boundary heat loss is allowed, it is now found that spatial variability is possible for any σ, but the pattern amplitude is determined by the value of γ.

It is natural therefore to ask what becomes of the patterns in Section 4 when heat loss at the boundary is allowed. Figures 6(a) and (b) illustrate the complex and surprising behaviour of the various solution branches in Figures 4 as the loss coefficient γ is increased, for a particular value $\sigma = 0.07$ of the chemical diffusion coefficient. There are essentially three different solution branches in these Figures, and to distinguish between them, they have been plotted using a solid line, a dashed line, and a dot-dashed line, for ease of viewing. Each solution branch contains at least one fold bifurcation, and the two branches drawn with the solid and the dashed lines both begin and end on the vertical axis $\gamma = 0$, so providing an analytic link between several of the solution curves shown in Figures 4.

Perhaps the most unexpected feature of the bifurcation diagrams in Figures 6 is that one of the solution branches, shown with a dot-dash line, appears to continue out to $\gamma \to \infty$, and numerical solutions have indeed been found for $\gamma = 150$. It was initially anticipated that a very large heat loss coefficient γ would simply give a flat temperature profile of very small amplitude, but it is evident from Figures 6 that such is not the case. Instead, the pattern is able to maintain a large amplitude, by allowing $T \to \theta_a$ as $r \to 1$ with very large negative slope $T'(r)$ in this region. In effect, a narrow thermal boundary layer is formed near $r = 1$, as $\gamma \to \infty$.

The complexity of pattern formation has been increased by allowing heat loss at the boundary $r = 1$, and to illustrate this point we present seven different temperature patterns, all for the same value of the loss coefficient $\gamma = 0.5$, in Figures 7. These profiles have been drawn using solid lines, dashed lines and dot-dashed lines, so as to enable them to be identified with the solution branches in Figures 6. Again it is seen that the non-linearity of the governing system (6) results in a rich choice of pattern behaviour, and the one that would be observed in an experiment would be strongly dependent on initial conditions.

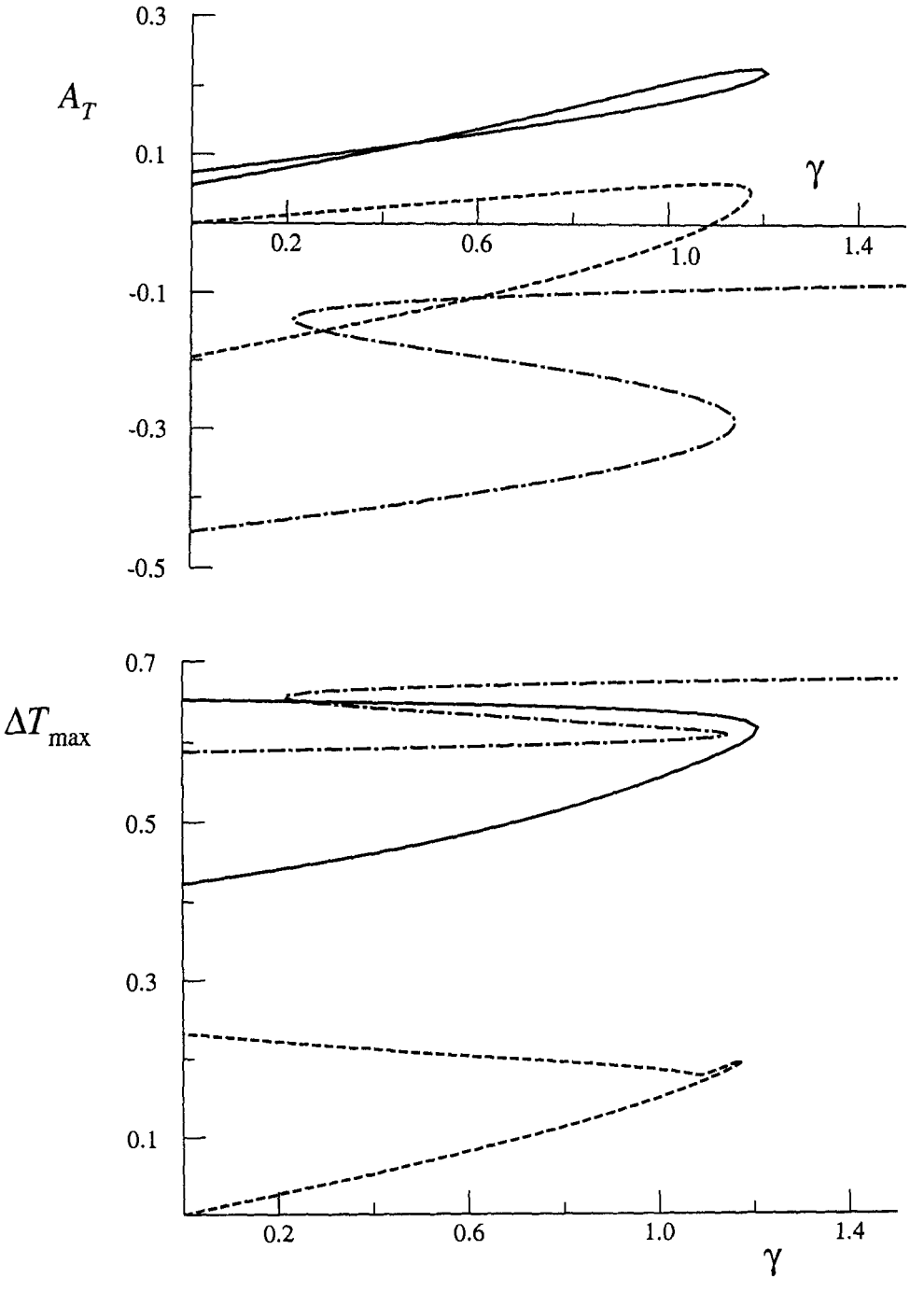

Fig. 6. Variation of pattern amplitudes (a) A_T and (b) ΔT_{max} with loss coefficient γ, for the second eigensolution. Here, $\beta = 1$, $\alpha = 0.001$, $\mu = 0.5$, $\theta_a = 0.18$, and $\sigma = 0.07$.

6. Conclusions

In this paper, both analytical and numerical methods have been used to study the formation of spatially dependent patterns in a burning reaction at the face of a substrate. The numerical

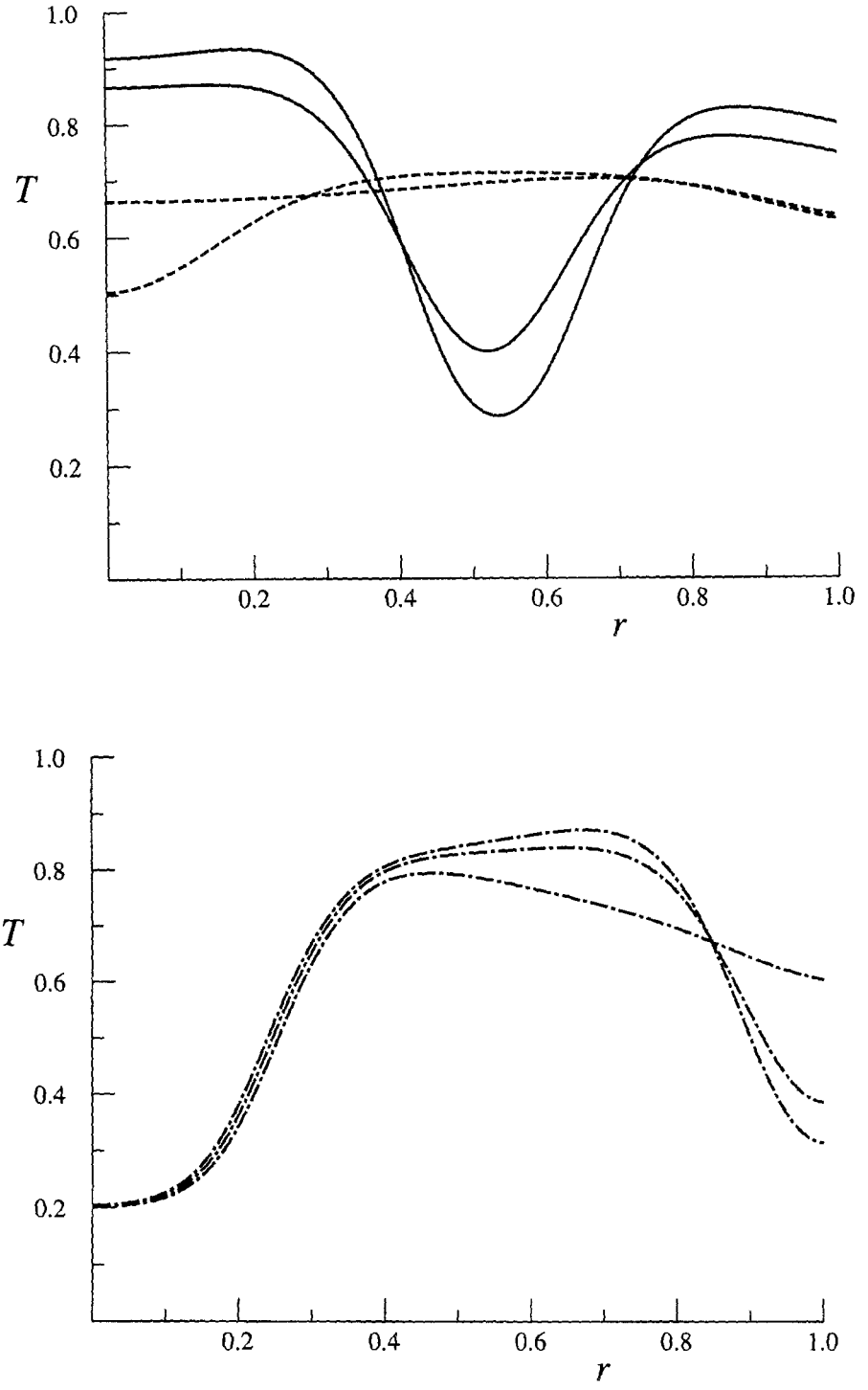

Fig. 7. (a) and (b). Seven different patterns, all obtained with the same loss coefficient $\gamma = 0.5$. The remaining parameters have the same values as for Figure 6.

results were based on the use of a highly efficient shooting scheme, which allowed a rather detailed exploration of the possibilities for pattern formation, and of the order of 700 separate converged numerical solutions have been used in this study.

Patterns are formed by Turing bifurcation from a homogeneous steady state, in the absence of mixing, and it is generally the case that only the first few eigenmodes give permissible patterns. Nevertheless, the bifurcation diagrams become extremely elaborate, primarily through repeated fold bifurcations, so that a multiplicity of patterns is possible for a given set of physical parameters. In addition, the points of Turing bifurcation themselves evidently possess a complicated structure, so that multiple solution branches can emanate from the one point. It has been found here that both the first and the second eigen-pattern can bifurcate from the Turing point corresponding to the first eigensolution.

This complexity of pattern formation behaviour is not removed by allowing heat dissipation at the boundary of the region, as might be expected, but is instead enhanced by it. This is perhaps consistent with the observation of Bayliss and Matkowsky [12] that chaotic time dependent behaviour may be observed in these cases.

The question of pattern selection naturally arises from this work, and it must be the case that, when such a multiplicity of solutions exists, the pattern which is actually observed is strongly influenced by initial conditions. Small perturbations in a laboratory experiment might also cause the pattern to jump from one of its possible steady states to another, so giving the appearance of a random or chaotic field.

References

1. I. Ye. Sal'nikov, Contribution to the theory of the periodic homogeneous chemical rections, *Zh. Fiz. Khim.* 23 (1949) 258–272.
2. B.F. Gray and M.J. Roberts, An asymptotic analysis of the Sal'nikov thermokinetic oscillator, *Proc. Roy. Soc. London, Ser. A* 416 (1988) 425–441.
3. L.K. Forbes, M.R. Myerscough and B.F. Gray, On the presence of limit-cycles in a model exothermic chemical reaction: Sal'nikov's oscillator with two temperature-dependent reaction rates, *Proc. Roy. Soc. London, Ser. A* 435 (1991) 591–604.
4. B.F. Gray and L.K. Forbes, Analysis of chemical kinetic systems over the entire parameter space IV. The Sal'nikov oscillator with two temperature-dependent reaction rates, *Proc. Roy. Soc. London, Ser. A* 443 (1994), 621–642.
5. P. Gray and J.F. Griffiths, Thermokinetic combustion oscillations as an alternative to thermal explosion, *Combust. Flame* 78 (1989) 87–98.
6. D.P. Coppersthwaite, J.F. Griffiths and B.F. Gray, Oscillations in the H_2 + Cl_2 reaction: Experimental measurements and numerical simulation, *J. Phys. Chem.* 95 (1991) 6961–6967.
7. R. Dillon, P.K. Maini and H.G. Othmer, Pattern formation in generalized Turing systems I. Steady-state patterns in systems with mixed boundary conditions, *J. Math. Biol.* 32 (1994) 345–393.
8. P. Gray and S.K. Scott, *Chemical Oscillations and Instabilities. Non-linear Chemical Kinetics*, Oxford: Clarendon Press (1990).
9. L.K. Forbes, One-dimensional pattern formation in a model of burning, *J. Austral. Math. Soc., Ser. B* 35 (1993) 145–173.
10. P. Gray and W. Kordylewski, Travelling waves in exothermic systems, *Proc. Roy. Soc. London, Ser. A* 416 (1988) 103–113.
11. A. Bayliss, B.J. Matkowsky and H. Riecke, Structure and dynamics of modulated traveling waves in cellular flames, *Physica D* 74 (1994) 1–23.
12. A. Bayliss and B.J. Matkowsky, From travelling waves to chaos in combustion, *SIAM J. Appl. Math.* 54 (1994) 147–174.
13. L.K. Forbes, On stability and uniqueness of stationary one-dimensional patterns in the Belousov-Zahbotinsky reaction, *Physica D* 50 (1991) 42–58.